Glud, J.A., Carraro, P.A., Quaresimin, M., Dulieu-Barton, J.M., Thomsen, O.T. and Overgaard, L.C.T., "A damage-based model for mixed-mode crack propagation in composite laminates", Composites A, 107, 2018, 421-431. https://doi.org/10.1016/j.compositesa.2018.01.016

A damage-based model for mixed-mode crack propagation in composite laminates

J.A. Glud[1], P.A. Carraro[2], M. Quaresimin[2], J.M. Dulieu-Barton[3,1] and O.T. Thomsen[3,1] and L.C.T. Overgaard[1]

[1]Department of Mechanical and Manufacturing Engineering, Aalborg University

Fibigerstraede 16, 9220, Aalborg Oest, Denmark

Email: {jag,ott,lcto}@m-tech.aau.dk, web page: www.m-tech.aau.dk

[2]Department of Management and Engineering, University of Padova

Stradella S. Nicola 3, 36100 Vicenza, Italy

Email: marino.quaresimin@unipd.it, web page: http://www.gest.unipd.it/en

[3]Faculty of Engineering and the Environment, University of Southampton

Highfield, SO17 1BJ, Southampton, United Kingdom

Email: {janice,o.thomsen}@soton.ac.uk, web page: www.southampton.ac.uk/engineering

Keywords: Laminates, Fatigue, Transverse Cracking, Mixed-Mode, Damage Mechanics, Multi-scale

Abstract

A model for the off-axis crack propagation in laminated fibre reinforced polymer composites subjected to multiaxial fatigue loadings is presented. On the basis of several observations reported in the literature, the crack propagation phenomenon can be seen as the result of a series of micro-scale events occurring ahead of the crack tip within a process zone. The mixed mode loading condition defines the type of the micro-scale events which occur in the process zone and lead to fatigue crack propagation. Based on this evidence and by using a multiscale approach to determine the micro-scale stress fields in the matrix, two simple parameters are defined for predicting the crack growth rate through a Paris-like law. By extracting the proposed

Glud, J.A., Carraro, P.A., Quaresimin, M., Dulieu-Barton, J.M., Thomsen, O.T. and Overgaard, L.C.T., “A damage-based model for mixed-mode crack propagation in composite laminates”, Composites A, 107, 2018, 421-431. https://doi.org/10.1016/j.compositesa.2018.01.016

parameters from experimental data obtained from the literature, it is demonstrated that the crack propagation data are all included into two Paris-like scatter bands covering the whole mode-mixity range.

1. Introduction

Laminated Fibre Reinforced Polymer (FRP) composites are used extensively for weight critical structural applications, which are often subjected to severe fatigue loading conditions over their service life. The fatigue loading conditions are typically non-proportional and multiaxial, making predictions of fatigue life difficult because of the influence of multiple factors that need to be combined. Therefore, many researchers have resorted to phenomenological models to make fatigue life predictions, which have been shown to be deficient when seeking safe design guidelines [1]. Therefore, physically based models that incorporate a better understanding of material behaviour are required to establish more consistent and generally applicable fatigue models, as well as more reliable design guidelines.

The sequence of damage modes for multidirectional laminates usually consists of off-axis cracking followed by delamination and fibre breakage leading to the ultimate structural failure [2–5]. Off-axis cracks are through-the-thickness cracks in the laminate layers, which propagate along the longitudinal direction in the matrix between the fibres. Off-axis cracking represents a very important progressive damage mode, because it usually occurs first, thus promoting other damage modes, such as delaminations and fibre failures; in addition, off-axis cracking is directly linked to the stiffness degradation observed in composite laminates [6]. Another important consideration is that the damage evolution in composite laminates is a multi-scale and hierarchical process, involving several length scales [7]. In fact, the initiation of an off-axis crack (or macro-crack) results from the damage accumulation in the matrix material at the micro-scale, i.e. at the length scale of the inter-fibre spacing [7]. A damage-based model for the initiation of off-axis cracks must therefore consider this evidence through a multi-scale approach.

A damage-based crack initiation criterion for multiaxial fatigue loading was presented in [8] where two micro-scale stress parameters controlling the initiation process were identified from experimental observations of damage modes occurring at the fibre-matrix level. Depending on the multiaxial stress state, either the Local Hydrostatic Stress (LHS) or the Local Maximum Principal Stress (LMPS) were found to promote the initiation of off-axis cracks. To use this model, two S-N curves for crack initiation must be derived from fatigue experiments. One curve should be derived for a stress state where the LHS is governing the crack initiation and the other should be derived when the initiation is driven by the LMPS.

When an off-axis crack has initiated within a ply of a laminate it will grow in a steady state manner along the fibre direction. The resistance to the crack propagation has been found to depend on the local mode-mixity in the off-axis crack front [5]. Typical results found in literature show that in terms of the total Energy Release Rate (ERR or G_{tot}), the resistance to fatigue crack growth in Mode I is less than in Mode II and the trend between the pure mode conditions is not necessarily monotonic. In spite of the importance of this phenomenon, physically based models targeted specifically at mixed-mode off-axis tunnelling crack propagation do not exist at present. However, a wide range of literature is available regarding the propagation of interface cracks in bonded joints and delaminations in laminates (e.g. [9–17]). In these cases, a macro-crack grows within a thin adhesive or matrix layer between the fibres. Therefore, in both these cases and in that of an off-axis crack, the problem can be regarded as that of a crack growing under mixed-mode conditions in a soft interlayer between the two stiffer adherends. Because of the analogy with adhesive bonds, a literature review of the modelling efforts related to the mixed-mode growth of delaminations and bond-line cracks is pertinent and may provide inspiration for the development of a new propagation criterion for off-axis tunnelling cracks. Several empirical relationships have been proposed to predict the critical ERR and the crack growth rate in fatigue as a function of the mode-mixity for inter-laminar cracks. Benzeggagh and Kenane [9] studied mixed-mode delamination propagation in glass/epoxy under quasi-static loading using the Mixed-Mode Bending (MMB) test fixture. Based on the experimental results, the authors computed the critical ERR for any mode-mixity using results for at least three different conditions to obtain the empirical constants of their proposed power law relationship. The same authors, later, proposed power law relationships for the proportional scaling coefficient and the slope of the Paris-like law to predict the crack growth rate (CGR) for varying mode-mixity [10], which required fatigue tests with at least three different mode-mixities to obtain the empirical constants. Liu et al. [11] used an MMB fixture to test bonded metal joints subjected to mixed-mode conditions and found that a linear interpolation between G_{Ic} and G_{IIc} was sufficient to predict the critical ERR for the mode-mixity range under consideration. Adhesively bonded double-lap joints were tested in [12], where a similar linear interpolation of the critical ERR was used to compute an equivalent ERR as input to a Paris-like law to predict the CGR. Adhesively bonded metallic joints were tested under quasi-static loading in [13] and under fatigue in [14] and purely empirical parabolic fits were used to provide the measured proportional scaling and the exponent of the Paris-like law. Even though the proposed empirical relationships have been reported to fit the reported experimental results, it is clear that, due to the empirical nature of the approach, several tests are required to derive the empirical constants. Moreover, it is not clear whether the derived empirical constants are valid for material systems other than those specifically studied.

Physically based models could potentially circumvent the need for multiple fatigue tests on a range of materials and provide more reliable predictions. However, there is little published on the observed damage mechanisms for interfacial fatigue crack propagation in the literature, so only few physically based models are available. For static loading, Liu et al. [11] reported two distinct types of fracture behaviour, which were found to depend on the mode-mixity. For Mode I dominated loading, a coplanar crack growth was observed, whereas for Mode II dominated loading shear cusps were observed ahead of the crack tip. This region of damage ahead of the crack tip is commonly referred to as the process zone [18]. The same characteristics of the crack path have been reported in [16,17,19] for fatigue loading as well. Based on the reported damage mechanisms for interfacial cracks, Wang [20] proposed a quasi-static fracture criterion that uses the Mode I ERR and a Drucker-Prager type parameter for predicting the critical ERR in the near Mode I and Mode II conditions, respectively. The two models for each type of fracture proposed by Wang [20] were shown to successfully predict the critical fracture toughness for a wide range of mixed-mode quasi-static load cases.

During static and fatigue loading, the damage evolution ahead of the crack tip does not appear to be a point phenomenon, and therefore the idea of a failure process zone model has received considerable attention. Several cohesive zone models and numerical approaches have been developed to create a unified approach for the initiation and propagation and to model the softening behaviour in the process zone through traction-separation laws. However, current methods for predicting the effect of mixed-mode loading rely on empirical relationships [15]. Inspired by the model presented in [20] and the experimental evidence indicating a finite region of damage for Mode II dominated loading reported in [16], Carraro et al. [18], proposed that the average Maximum Principal Stress in a finite region of the adhesive ahead of the crack tip governs the crack propagation in bonded joints for both static and fatigue loading. Finite Element (FE) analyses were adopted to compute the average Maximum Principal Stress in a control volume representative of the process zone, with the adhesive modelled as an undamaged continuum. It was shown that the model allows the fatigue CGR data for Mode II dominated loading to be represented in a single scatter band, when a fixed size of the finite failure process zone was chosen (three times the adhesive thickness). The Mode I ERR contribution was shown to collapse the CGR data for Mode I dominated loading in a single scatter band, hence enabling the CGR in the full mode-mixity range to be described by two Paris-like master curves. The result is a model that, though requiring some computational effort, only requires experimental data for two different mode-mixities (i.e. pure Mode I and Mode II) to derive the coefficients of the two Paris-like master curves.

As mentioned above, off-axis tunnelling cracks have not been widely covered in the literature, meaning that an off-axis crack propagation model suitable for structural scale analysis is highly desirable. To achieve this ambitious target, an efficient multi-scale strategy along with a damage-based mixed-mode model is required. A new damage-based model is developed and it is shown that two Paris-like master curves and scatter bands can be adopted to predict the CGR for the entire range of mode-mixities. As a consequence, data from fatigue tests on only two different laminate configurations are required as input. Furthermore, a novel multiscale approach is devised, where the model calculates the micro-scale parameters adopted for the predictions using information obtained from the larger scales, resulting in computationally efficient predictions suitable for structural scale analysis.

2. Crack propagation mechanisms

As already mentioned, when a crack propagates in a soft matrix layer between stiffer adherends, as in the case of inter-laminar and also tunnelling cracks, two main mechanisms can be observed at the micro-scale, depending whether the loading condition is Mode I or II dominated. As reported in [11,16–19], the propagation of an inter-laminar crack under near mode I conditions occurs in a co-planar manner at the interface or within the matrix inter-layer, as shown in Figure 1a). In particular, if the interface is weaker than the matrix, a self-similar propagation will occur at the interface. This scenario is typical of pure Mode I conditions, but it was observed also in the presence of small Mode II contributions [5,16,18]. Therefore, the

Mode I ERR (G_I) is responsible for the co-planar crack growth propagation, when the Mode II ERR (G_{II}) contribution is sufficiently low, as discussed extensively in [11,18]. Consequently, predictions of the CGR for the co-planar propagation condition can be done based on G_I only. For the case where the interface is tougher than the matrix, scarps and ribbons are the most commonly observed fractographic features in FRP materials [19,21]. Figure 1a) illustrates the series of events that cause these features. Micro-voids develop in the process zone and are initially separated from the macro-crack. It is reasonable to postulate that the micro-voids occur where weak spots are located in the process zone. Weak spots could be pre-existing micro or nano voids or flaws, or regions with a lower matrix strength due to an imperfect curing. Such a process zone typically remains constrained in the matrix layer where the macro-crack is situated because of the constraining effect of the fibres. Figure 1a) shows under mode Mode I loading the scarps, which form from the coalescence of micro-voids growing at different planes ahead of the crack tip, and ribbons resulting from the coalescence of overlapping micro-cracks. Then, the scarps or ribbons coalesce with the macro crack and cause the crack to propagate. These cavitation-like phenomena are typical of Mode I dominated loadings [19,21] and it is reasonable to assume that they are controlled by the hydrostatic stress component ahead of the crack tip, which is very high for Mode I loading. The series of events shown in Figure 1a) has been confirmed in [5], where the fracture surfaces of glass/epoxy tubes under Mode I dominated conditions showed both the presence of clean fibres and scarps and ribbons in the matrix, indicating that both the adhesive and the cohesive types of propagation could potentially occur for tunnelling cracks.

A different damage scenario was observed for Mode II dominated loading conditions [11,16–19] and is illustrated in Figure 1b). In this case the crack initially grows within the matrix layer along the Mode I dominated direction, which is at an inclined angle compared to the crack plane. However, the crack can only grow in this direction until it is close to the adherends or the fibres, which prevent the further propagation in this direction. This is also the case for off-axis tunnelling crack propagation in FRPs, where the crack propagates in the matrix and the fibres act as a constraining layer, which prevent the crack from propagating in the Mode I favourable direction. Consequently, the crack advances through the initiation of multiple tilted layered cracks (micro-cracks) ahead of the crack tip. Initially these micro-cracks are separated from the main crack, which implies that the stress state ahead of the crack tip in the process zone must play an important role in the damage progression. As the shear band limit is approached, the individual micro-cracks grow together with the macro-crack and result in a rough fracture surface with the presence of shear cusps [5], as shown in Figure 1b). As discussed in [11,17] and validated by FE analyses in [18], the evolution of this damage mode is controlled by the maximum principal stress within the matrix, ahead of the crack tip. This scenario was observed in [7] during the fatigue propagation of 45° off-axis cracks in a glass/epoxy laminate, where in a small region ahead of the crack tip (process zone) micro-cracks, inclined with respect to the fibres, initiated. Furthermore, also in the case of tunnelling cracks, for Mode II dominated loading the crack propagation is controlled by the maximum principal stress in the matrix ahead of the crack tip.

To conclude, for interface crack propagation under Mode I dominated loading, it is well established in the literature that G_I can be used for predicting the CGR. Under loading conditions that are not Mode I dominated then a new damage-based criterion is required that utilises the micro-scale stress fields in the matrix in the neighbourhood of the crack tip, in particular the hydrostatic and the maximum principal stresses. In the next section, the multi-scale approach adopted for predicting the propagation rate in these conditions is presented.

3. Multi-scale modelling

The concept of the multi-scale modelling proposed in the following is illustrated in Figure 2. First, the analysis at the structural scale is carried out to determine deflections, strains and stresses at the laminate level. Second, a macro-scale analysis is carried out using the Classical Lamination Theory (CLT) to obtain stresses and strains in the material coordinate system of the constituent layers. In the presence of off-axis cracks in these layers, several approaches can be adopted for modelling the laminate response both in terms of global and ply-level stresses and strains. In [6] the available analytical, semi-analytical or numerical tools are reviewed alongside with the application of an *optimal shear-lag analysis* to general laminates. These models can also be adopted for the estimation of the Mode I and Mode II ERR components associated to a propagating crack. Third, the micro-scale analysis is performed for the calculation of the local stress fields in the matrix ahead of the macro-crack tip. As shown later, these stress fields are obtained by starting with the ERR components from the macro-scale analysis.

3.1 Macro-scale stress fields

At this scale the plies of a laminate are considered as homogeneous materials having orthotropic apparent elastic properties. Accordingly, by defining the material reference system as shown on right hand side in Figure 2, the constitutive law can be written as

$$\begin{Bmatrix} \epsilon_{xx} \\ \epsilon_{yy} \\ \epsilon_{zz} \\ \gamma_{yz} \\ \gamma_{xz} \\ \gamma_{xy} \end{Bmatrix} = \begin{bmatrix} S_{11} & S_{12} & S_{13} & 0 & 0 & 0 \\ S_{21} & S_{22} & S_{23} & 0 & 0 & 0 \\ S_{31} & S_{32} & S_{33} & 0 & 0 & 0 \\ 0 & 0 & 0 & S_{44} & 0 & 0 \\ 0 & 0 & 0 & 0 & S_{55} & 0 \\ 0 & 0 & 0 & 0 & 0 & S_{66} \end{bmatrix} \begin{Bmatrix} \sigma_{xx} \\ \sigma_{yy} \\ \sigma_{zz} \\ \tau_{yz} \\ \tau_{xz} \\ \tau_{xy} \end{Bmatrix} \quad (1)$$

The presence of a crack in an anisotropic plate causes a stress singularity close to the crack tip, of which the value is equal to 0.5 [22]. After re-arranging the equations presented by Sih-Irwin-Paris [22], the plane strain asymptotic stress fields along the crack bisector ($\theta = 0$) can be written as

$$\begin{aligned} \sigma_{xx} &= \frac{K_I}{\sqrt{2x}} \cdot s_1 \cdot s_2 \\ \sigma_{yy} &= \frac{K_I}{\sqrt{2x}} \\ \tau_{xy} &= \frac{K_{II}}{\sqrt{2x}} \\ \sigma_{zz} &= -\frac{S_{31}\sigma_{xx} + S_{32}\sigma_{yy}}{S_{33}} \end{aligned} \quad (2)$$

where σ_{xx}, σ_{yy} and τ_{xy} are the longitudinal, transverse and in-plane shear stresses, respectively, σ_{zz} is the through-the-thickness stress, x is the distance from the crack tip, K_I and K_{II} are the Mode I and Mode II Stress Intensity Factors (SIFs) and s_1 and s_2 are given as

$$s_{1,2} = \sqrt{-\frac{-(2B_{12}+B_{66}) \pm \sqrt{(2B_{12}+B_{66})^2 - 4B_{11}B_{22}}}{2B_{11}}} \quad (3)$$

where B_{ij} are the reduced elastic constants under plane strain conditions [22], which read as

$$B_{ij} = S_{ij} - (S_{i3} \cdot S_{j3})/S_{33} \quad (4)$$

As off-axis cracks propagate along the fibre direction, the crack plane coincides with an orthotropy plane, so that the Mode I and Mode II contributions are decoupled. In this condition, the following relationships exist between the SIFs and the ERR components [22]:

$$K_I = \sqrt{\frac{G_I}{\pi}\left[\sqrt{\frac{B_{11}B_{22}}{2}}\left(\sqrt{\frac{B_{22}}{B_{11}}}+\frac{2B_{12}+B_{66}}{2B_{11}}\right)^{\frac{1}{2}}\right]^{-1}}$$

$$K_{II} = \sqrt{\frac{G_{II}}{\pi}\left[\frac{B_{11}}{\sqrt{2}}\left(\sqrt{\frac{B_{22}}{B_{11}}}+\frac{2B_{12}+B_{66}}{2B_{11}}\right)^{\frac{1}{2}}\right]^{-1}} \quad (5)$$

The Sih-Irwin-Paris solution (identified as S-I-P in the following) is valid for a 2D problem. In principle, the propagation of a crack in a layer within a laminate is a 3D problem, as the crack is constrained by the adjacent plies. However, the possibility of considering a 2D approach as a simplifying assumption is explored in the following, as this is an important step in determining the local stress fields at the micro-scale. To this end, a dedicated Finite Element (FE) analysis was carried out. A 3D unit-cell model of a $[0/90_3/0]$ laminate, similar to that reported in [5], was created to study the stress field in the process zone, with UD constraining layers. The material properties for the model are given in Table 1. A sketch of the model is provided in Figure 3, showing that for Mode I loading the displacement Boundary Condition (B.C.) was chosen as $\frac{U_y}{L} = 0.1 = \epsilon_{yy}$, and for pure Mode II loading the displacement B.C. was chosen as $\frac{2U_x}{L} = \frac{4U_y}{W} = 0.1 = \gamma_{xy}$. In [23] it has been shown that the ERR in the crack front becomes independent of the crack length and the crack front geometry, when the off-axis crack reaches a certain length, (usually at a length of ~2 times the layer thickness). Therefore, the crack length, *c,* was chosen as *L/2*, to be in the steady state regime. The geometry was selected such that the influence of edge effects could be ignored, which was achieved by choosing $L = W = 6$ mm (see Figure 3). The crack front was modelled as straight. FE analyses were carried out using the commercial code ANSYS® 15.0. 8-noded 'Solid 185' elements were used throughout and the thickness of the cracked layer was divided in 20 elements. Only mapped meshing was used in the FE model and the mesh was constructed such that it became increasingly finer as the crack tip was approached. The element side length at the crack tip was $2.7 \cdot 10^{-4}$ mm. The J-integral function of ANSYS® was used to compute the ERR for each node in the crack front and convergence was obtained at the 2nd contour. The stresses along the crack bisector plane (as a function of *x*) were extracted from the model using 20 interpolation paths covering the entire layer thickness.

Material UE 400-REM – CIT Composite Materials Italy					
E_1 [GPa]	E_2 [GPa]	ν_{12}	G_{12} [GPa]	V_f	Thickness [mm]
34.9	9.4	0.33	3.23	55%	0.38

Table 1: Material properties from [5,8] used for FE analysis.

The stress fields obtained from the FE model along the crack plane ahead of the crack tip, averaged along the 90° ply thickness, are plotted in Figure 4 for both pure Mode I and II loadings. It should be noted that the crack plane coincides with a symmetry plane for the pure Mode I loading case, and with an anti-symmetry plane for the Mode II loading case. Consequently this means that for the symmetric Mode I opening case the shear stress components τ_{xy} and τ_{yz} must be zero along the considered path, while the normal stress components and τ_{xz} must be zero along the path for the Mode II case. The stresses along the interpolation paths are compared in Figure 4 with the stresses predicted by the S-I-P equations, valid for a plane strain stress state [22], to which the far field stresses, obtained from the CLT, were added as a constant term. The SIFs used in the S-I-P equations were computed using Eq.(5) and the ERR obtained from the FE model using the J-integral approach for each node in the crack front. It is important to note that, in the case of a tunnelling crack, the ERRs and therefore the SIFs do not depend on the crack length as the propagation occurs in a steady state regime. The stress field predicted by the S-I-P solution was then computed for each node and subsequently averaged as $\sigma_{avg} = \frac{1}{t_k}\int_{-t_k/2}^{t_k} \sigma(z)dz$.

The failure process zone, as reported in [7], is at the scale of the inter-fibre distance, which is approximately 2-5 μm. It is clear from Figure 4, that the influence of the out-of-plane shear stresses is negligible in the region from the crack tip to about 5μm ahead of the crack tip (near the crack tip region), since these stresses are two orders of magnitude less than the non-zero in-plane stress components. From Figure 4 it is also observed that the S-I-P solution shows reasonably good agreement with the FE results, which indicates that the plane strain assumption is valid. The relative difference between the S-I-P and the 3D FE solutions increases beyond the near tip region due to the constraining layer effect, which makes the FE solution converge faster to the far field stress. As a conclusion of this analysis, it is possible to say that the stress state in a constrained layer in the neighbourhood of the tips of tunnelling cracks can be considered as close to a plane strain condition. In addition, the S-I-P equations can be adopted for the through-the-thickness stresses when the SIFs are calculated from the ERR components estimated via FE analyses or other analytical or semi-analytical models, as those revised in [6].

3.2 Micro-scale stress fields

From the macro-scale analysis it was possible to extract the ply-level stresses at the crack front, which confirmed the plane strain assumption made before. However, the main outcome is the value of the Mode I and II ERRs associated to a given geometry and loading condition. These can be calculated via FE models or, as already mentioned, by one of the analytical models available in the literature. It is important to state that all the methods mentioned above for calculating the ERR components consider the plies to be homogeneous and orthotropic. This approach is valid only if the crack is long compared to a characteristic length, which in this case must be related to the material microstructure. Therefore, the characteristic length is related to the reinforcement fibre diameter or the average distance between neighbouring fibres, rather than the layer thickness. To determine when an off-axis crack can be considered as long compared to the material micro-structure, FE analyses were carried out. A homogenous cracked plate was compared to a heterogeneous lamina where the reinforcement and matrix materials were modelled separately. To simplify the problem from a computational point of view, 2D plane stress analyses were carried out. Thus, in the heterogeneous model, the fibres were not modelled with a circular cross section but rather as rectangular areas in the x-y plane, as shown in Figure 5a). However, this will not influence the validity of the conclusions that are drawn later concerning the minimum allowable crack length for the application of the homogenisation technique in the ERR calculation. The material properties adopted in the analyses are given in Table 2. The rule of mixtures was used to compute the homogenised properties starting from those of the constituents, considering a volume fraction of 0.5. A sketch of the FE model with the imposed B.C. for Mode I and II loadings, where $N_y = N_{xy} = 50\frac{\text{N}}{\text{mm}}$, is shown in 5b) and c). The geometry of the lamina plate was chosen so that $L = W = 16$ mm. In the heterogeneous model the crack was positioned in the middle of the resin layer at the centre of the plate width. Mapped meshing was used in the model and the mesh was constructed such that it became increasingly finer closer to the crack tip; the element side length at the crack tip was $2.5 \cdot 10^{-5}$ mm. The J-integral function of ANSYS® was used to compute the ERR at the crack tip and convergence was obtained at the 7$^{\text{th}}$ contour.

Glass Fibre		**Epoxy**		**Homogenised Properties**			
E_f [GPa]	V_f	E_m [GPa]	V_m	E_1 [GPa]	E_2 [GPa]	G_{12} [GPa]	ν_{12}
70	0.22	3.2	0.37	36.6	6.1	2.9	0.30

Table 2: Material properties used for the FE analysis of the lamina plate models.

To determine if the crack length is sufficiently large for the homogenisation technique to be valid, the relative error between the homogeneous and the heterogeneous models was computed as function of the crack length for both Mode I and Mode II loading. The results are shown in Figure 6a). It can be observed that the relative error between the ERRs for the homogeneous and heterogeneous material models converges asymptotically to a fixed value for Mode I loading, whereas for the Mode II load case the relative error converges to zero. The reason for the fixed error of about 6% for the Mode I case is due to the use of the rule-of-mixture formula for determining the homogenised properties, which provide an estimate of the transverse Young's modulus E_2 that is too compliant and results in a higher ERR in the homogeneous than in the heterogeneous material model. It is further observed from Figure 6a) that the ERR for both loading conditions have converged at approximately 40 times the inter-fibre distance, t_m. This means that the ERR can be computed through a homogenous model when the off-axis crack is 40 times longer than the characteristic length. For the present case, where the characteristic length is 2-5μm, the crack length should be in the range 0.08-0.2 mm, hence the material can be treated as homogenous. At this point, it should be considered that the aim of the present work is to describe the steady state propagation of off-axis cracks, which happens when they are ~2 times longer than the ply thickness [24]. Therefore, it can be concluded that a homogeneous model can be adopted for the calculation of the ERR components for tunnelling cracks.

Therefore, for steady state tunnelling cracks, the following equations hold valid:

$$G_{I,Hom} = G_{I,Het} = G_I \tag{6}$$

$$G_{II,Hom} = G_{II,Het} = G_{II} \tag{7}$$

where subscripts *Hom* and *Het* denote the homogeneous and heterogeneous models, respectively.

Eqs. (6) and (7) provide an essential result for the computation of the local stress fields in the matrix. Considering the coordinate system shown in Figure 7, the asymptotic stress fields in the matrix along the crack bisector, under a plane strain assumption, can be written through the Irwin equations, valid for isotropic materials

$$\begin{aligned} \sigma_{xx} &= \sigma_{yy} = \frac{K_{I,m}}{\sqrt{2\pi x}} \\ \tau_{xy} &= \frac{K_{II,m}}{\sqrt{2\pi x}} \\ \sigma_{zz} &= 2\nu_m \frac{K_{I,m}}{\sqrt{2\pi x}} \end{aligned} \quad (8)$$

where ν_m is the matrix Poisson's ratio and $K_{I,m}$ and $K_{II,m}$ are the local SIFs in the matrix. Therefore, the micro-scale stress fields in the matrix can be calculated once the local SIFs are known. Through the equivalences in Eqs. (6) and (7), they can be expressed as

$$K_{I,m} = \sqrt{\frac{G_I \cdot E_m}{(1-\nu_m^2)}} \quad (9)$$

$$K_{II,m} = \sqrt{\frac{G_{II} \cdot E_m}{(1-\nu_m^2)}} \quad (10)$$

where E_m is the matrix Young's modulus.

To validate the approach described in the above and show that the homogeneous isotropic material plane strain assumption is valid, the stress fields in the matrix were calculated using Eq. (8), with the SIFs estimated using Eqs. (9) and (10) and compared to the results along the crack bisector obtained with the FE analyses of the described 2D lamina model. This comparison is shown in Figure 6b, where there is good agreement between the analytical and numerical solutions within a distance of $\frac{t_m}{10}$ (marked with a red dashed line), with a slight departure in solutions between $\frac{t_m}{10}$ and t_m. Beyond this distance, higher order terms, depending on the local geometry and the elastic properties of the fibres, start to influence the stress fields significantly.

4. Definition of a crack propagation criterion

As described in section 3, the stress fields at the micro-scale in the matrix in the neighbourhood of an off-axis crack tip can be calculated through the following steps:

1) Structural scale analysis: the displacements and the laminate stresses and strains are calculated in the whole structure or component;

2) Macro-scale analysis: starting from the laminate stresses and strains, the Mode I and II ERRs are calculated through FE analyses or using one of the analytical models available in the literature;

3) Micro-scale analysis: starting from the ERR components calculated at the previous step, the stress fields in the matrix are calculated using Eq. (8), where the SIFs are estimated by means of Eq. (9) and (10).

As discussed in section 2, knowing the micro-scale stress fields in the matrix is essential for defining a propagation model that accounts for the mechanisms occurring during a cohesive type crack growth. In particular, close to pure Mode I conditions, the hydrostatic stress in the matrix can be seen as responsible for the cavitation induced void formation in the process zone. Under Mode II dominated loading, the maximum principal stress in the matrix is responsible for the initiation of the inclined cracks of which the coalescence results in a macro-crack propagation. With reference to the coordinate system shown in Figure 7, the intensity of the hydrostatic and maximum principal stresses in the matrix along the crack bisector plane, close to the crack tip, can be quantified by the following parameters:

$$K_h = \lim_{x\to 0}\left(\sqrt{2\pi x}\left[\frac{\sigma_x+\sigma_y+\sigma_z}{3}\right]\Big|_{\theta=0}\right) = \frac{2(1+\nu_m)K_{I,m}}{3} \tag{11}$$

$$K_p = \lim_{x\to 0}\left(\sqrt{2\pi x}\left[\frac{\sigma_x+\sigma_y}{2}+\sqrt{\left(\frac{\sigma_x-\sigma_y}{2}\right)^2+\tau_{xy}^2}\right]\Bigg|_{\theta=0}\right) = K_{I,m}+K_{II,m} \tag{12}$$

Substituting Eqs. (9) and (10) within Eqs. (11) and (12) and introducing the mode-mixity parameter $MM=G_{II}/(G_I+G_{II})$, it is possible to write the following relationships between the hydrostatic and maximum principal stress SIFs, K_h and K_p, and the ERRs calculated at the macro-scale:

$$K_h = \frac{2(1+\nu_m)}{3}\sqrt{\frac{G_I\cdot E_m}{(1-\nu_m^2)}} \tag{13}$$

$$K_p = \left(\sqrt{1-MM} + \sqrt{MM}\right)\sqrt{\frac{(G_I+G_{II})E_m}{(1-\nu_m^2)}} \qquad (14)$$

It can be seen that K_h depends on the Mode I ERR only, whereas K_p depends on the total ERR (G_I+G_{II}) and the mode-mixity. To comply with the notation used in most of the literature, i.e. adopting the ERR instead of the SIF for composite materials, G_h and G_p are defined as follows:

$$G_h = K_h^2\frac{(1-\nu_m^2)}{E_m}\frac{3}{2(1+\nu_m)} = G_I \qquad (15)$$

$$G_p = K_p^2\frac{(1-\nu_m^2)}{E_m} = \left(\sqrt{1-MM} + \sqrt{MM}\right)^2 \cdot (G_I + G_{II}) \qquad (16)$$

where K_h and K_p are taken from eqs. (13) and (14). Therefore, based on the mechanisms occurring during the propagation of an inter- or intra-laminar crack, it is possible to assume that the ERRs defined in Eqs. (15) and (16) can be used to predict the CGR under Mode I and Mode II dominated loading conditions, respectively. As mentioned in section 2, the propagation under near Mode I conditions can be of a cohesive or adhesive type. It is important to note that, independent of the type of propagation, the Mode I ERR is responsible for the crack advance in both cases.

In the present work it is suggested that the fatigue tunnelling crack propagation can be described by only two Paris-like scatter bands, covering the full range of mode-mixities. In particular, from MM = 0 to a certain threshold value MM^*, the Paris-like curve is expressed in terms of G_I. Conversely, for $MM>MM^*$ up to MM=1 (pure Mode II), G_p should be used. The transition value MM^* depends on the materials involved; for instance it will be shifted towards 1 if the interface is weak or the material is particularly prone to cavitation with respect to micro-cracking due to the principal stresses, and vice-versa. A more detailed discussion on how to calculate or estimate this value is provided in the next section.

A further feature of note is that Figure 5a shows that the micro-scale matrix stress fields were calculated adopting a schematic where it is assumed that the crack is placed in the middle of the matrix inter-layer. This is of course a simplification, as in reality the crack path is very complex with the tip continuously changing its position from the matrix to the interface in a way that is impossible to treat in a deterministic and efficient way. In the next section of the paper the model is a applied to several cases, the results of which show good correlation with experimental data. The conclusion being the simplifying assumption is sound and the physics of the phenomena can be captured using the model shown in Figure 5a.

5. Model validation

To illustrate the general applicability of the model developed in the preceding sections, several data sets from the literature were analysed using Eqs. (15) and (16). The only data set available in the literature, where the CGR for off-axis cracks was reported for more than three mixed-mode loading conditions is for glass epoxy tubes [5]. Therefore, thanks to the analogy with delaminations discussed in section 1, the model was applied to the off-axis crack propagation data from the mentioned tubes and then to delaminations in 0°/0° layer interfaces in both glass and carbon epoxy laminates.

The CGR data for glass-epoxy tubes from [5] are plotted in terms of G_{tot} in Figure 8a). The maximum cyclic value of the ERR is adopted in all the figures shown in this section. In Figure 8, each point in the plot represents a single crack propagating in a steady state manner, i.e. with a constant ERR and therefore a constant CGR, as explained in [5]. It can be seen that the energy required for the crack propagation increases with the mode-mixity. In fact, different Paris-like curves can be defined for different MM values. Instead, when the CGR is plotted as a function of G_I ($CGR = C \cdot G_I^n$, where C and n are empirical constants obtained by fitting the function to experimental data), for $MM = [0; 0.24]$ and G_p ($CGR = C \cdot G_{eq,p}^n$) for $MM = [0.24; 1]$, all the data fall inside two scatter bands as shown in Figure 8b) and c), where the relevant 95%-5% probability range is also reported. The range of the prediction interval for G_I is similar to the inherent scatter in the measured crack growth rates. This proves that the CGR under mixed-mode loading is accurately modelled by a single Paris-like law for $MM = [0; 0.24]$. The deviation obtained from the prediction interval for G_p is slightly larger than the inherent deviation in the measured CGR. However, the prediction interval for G_p is considerably smaller than for G_{tot} and therefore it can be concluded that a single Paris-like curve in terms of G_p can be used to describe the CGR for $MM = [0.24; 1]$. Based on the data, it is clear that data points for $MM = 0.24$ fall within the prediction interval for both models, indicating that the threshold values

*MM** should be around this value. This implies that the damage mechanisms connected with both the G_I and G_p models should occur. A transition between damage modes at this mode-mixity value is in agreement with the observations of the fracture surfaces reported in [5], where a change in the micro-scale damage mode was observed for *MM* higher than 0.24. It is interesting to make a consideration on the macro-scale stress fields close to the crack front. Using the S-I-P equations for calculating the asymptotic trends of the transverse stress σ_{yy} and the shear stress τ_{xy} for the mixed-mode condition of $MM = 0.24$, results in a bi-axiality ratio $\lambda_{12} = \frac{\sigma_6}{\sigma_2}$ =0.8. This value is within the transition zone found, for the same material, for the crack initiation phenomenon, which was shown to occur with similar mechanisms, related to the hydrostatic and principal stresses at the micro-scale [8]. The fact that *MM** is around a value of 0.24 is also consistent with the observations of damage modes in film epoxy adhesives as reported in [25]. Both scarps and tilted layered cracks aligned with the direction of the maximum principal stress for $MM = 0.20$ were observed, indicating that damage mechanisms associated with the hydrostatic stress and maximum principal stress were both active for this mode-mixity [25]. Based on the change in the damage mode observed at the microscopic scale and the fact that the model is able to collapse CGR data into one scatter band for each damage mode, it is concluded that the mechanics of crack propagation of off-axis cracks are modelled at a sufficient level of detail.

Other crack propagation data on glass/epoxy tubes were reported by Quaresimin et al. in [26] for additional load ratios *R* equal to 0.5 and -1. In the case of *R* = 0.5 the same mechanisms reported for *R* = 0.05 were observed, whereas no clear indications were obtained for tension-compression loadings. Accordingly, the proposed propagation model is applied to the data relevant to *R* = 0.5. In this case, only the pure Mode I condition falls within the range in which the propagation is Mode I dominated. However, it can be seen that a single scatter band can be defined in terms of G_p for *MM* = 0.56 and 0.84 (Figure 9).

As mentioned in the introduction, the problem of the tunnelling propagation of an off-axis crack is basically similar to that of an inter-laminar crack propagating in a 0°/0° interface. For this reason, CGR data for delaminations in unidirectional laminates were used to make an additional validation of the model. It should be noted that the model is only intended for problems where the failure process zone is small (2-5μm). Delaminations may have a large fracture process zone due to fibre bridging. Therefore, the model has only been applied to experimental delamination data from literature where the respective authors do not report extensive fibre bridging across the crack surfaces. In [10], delaminations in glass-epoxy laminates subjected to fatigue loading were studied for different mode-mixities, using Double Cantilever Beam (DCB) tests for Mode I loading, MMB tests for mixed-mode loading and the End-Loaded Split (ELS) tests for Mode II loading. The data from [10] are presented in Figure 10 along with Paris-like fits and 5%-95% probability scatter bands. The Paris-like law in terms of G_p has been fitted to CGR data for $MM = [0.28; 0.91]$, Figure 10c). The range of the prediction interval for the G_p Paris-like law is similar to the scatter in the material data, confirming the suitability of G_p to predict the CGR in the mode-mixity range given by $MM = [0.28; 0.91]$. This indicates that the transition zone between the damage modes is similar to that of the glass/epoxy material adopted for the tubes. The data for $MM = 1$ were not included in the fit shown in Figure 10c), as they appear as clear outliers with respect to other data. One possible reason is that these results were derived using ELS specimens, which results in compressive stresses on the crack surfaces. For off-axis cracks, such a stress state has been found to possibly alter the damage mechanisms leading to crack propagation [26]. Therefore, a possible limitation of the proposed model is that it is only applicable in the case of non-compressive stresses on crack surfaces. In Figure 10b) the CGR data are plotted as a function of G_I for $MM = [0; 0.28]$, showing, again, that they are all included in the same scatter band.

In Figure 11 the CGR data for a carbon/epoxy laminate [27] are shown. Apart from the pure Mode I condition, all the mode-mixity values relate to the G_p-controlled crack propagation. Figure 11c) shows the G_p Paris-like law fitted to the CGR data for the mode-mixity range given by $= [0.42; 1]$. The obtained scatter band is narrow compared to Paris-like plots in terms of G_{tot}. In fact, the range of the prediction interval in terms of G_p is similar to the scatter in the material data, confirming that this parameter is capable of describing mixed-mode propagation rates for $MM = [0.42; 1]$ for the material tested in [27] also. As only pure Mode I data is available for the G_I-controlled propagation, it is impossible to draw any conclusion on the transition value of the mode-mixity for the material tested in [27].

The inter-laminar crack propagation in carbon/epoxy laminates was also analysed in Refs [28–30], under pure Mode I [28], pure Mode II [29] and mixed-mode loadings [30]. The same material was tested in the three mentioned works. The Paris-like curves in terms of the total ERR are reported in Figure 12a), whereas

Glud, J.A., Carraro, P.A., Quaresimin, M., Dulieu-Barton, J.M., Thomsen, O.T. and Overgaard, L.C.T., "A damage-based model for mixed-mode crack propagation in composite laminates", Composites A, 107, 2018, 421-431. https://doi.org/10.1016/j.compositesa.2018.01.016
the plots in terms of G_I and G_p are shown in Figures 12b) and c) for *MM*= [0;0.2] and *MM* = [0.2; 1], respectively. Again, it can be seen that only two scatter bands include the crack propagation data for the whole mode-mixity range, and also for this material, the transition appears to be around *MM* = 0.2.

It has been shown in this section that the proposed criterion for the mixed mode crack propagation in composite laminates has been validated with a reasonable level of confidence. Moreover, it has been shown that the CGR data for the whole mode mixity range can be included in two scatter bands only, to be used when the propagation is G_I-dominated (MM from 0 to MM*) or G_p-dominated (MM from MM* to 1). As a consequence, the entire experimental characterisation of the fatigue crack propagation for several mixed mode conditions (resulting in a time-consuming campaign that requires the use of an MMB testing fixture) is no longer necessary. Thus, the crack propagation behaviour can be fully characterised once pure Mode I (DCB) and pure Mode II (ENF) tests have been carried out. Following this, the pure Mode I Paris-like curve in terms of G_I and the pure mode II curve in terms of G_p can be adopted for the prediction of the CGR for any mixed mode condition, for MM lower and higher than MM*, respectively.

The above leads to the final remaining question is on estimation of the transition value MM*. Once the two Paris-like curves, in terms of G_I and G_p, are known, it is a straightforward matter to draw constant-CGR curves (G_{tot} versus MM) as those shown in Figure 13 for the material system relevant to the data given in Figure 8. The transition value MM* is represented by the point where the curves obtained with the G_I- and G_p-related predictions intersect. In general, MM* will change slightly with the CGR. However, a limited interval can be identified (around MM* = 0.25 in this case) where the two criteria provide very similar predictions for the G_{tot} relevant to a given CGR or, vice-versa, for the CGR, given a G_{tot} value. Therefore, in this limited interval, of which the extension can be deduced by the constant–CGR plots, both criteria can be adopted, and the central value of the interval can be considered as the MM*.

6. Conclusions

A new damage-based model for mixed-mode crack propagation in composite materials has been developed. The principle behind the model is that the crack propagation process consists of a series of micro-scale damage events within a process zone ahead of the crack tip, occurring because of the presence of high local stresses in the matrix. A multiscale approach has been proposed for the calculation of such micro-scale stress fields as a first step for the definition of the new propagation model. From a review of fracture surfaces, it was evident that the mechanism of crack propagation changes when moving from a Mode I to a Mode II dominated loading condition. On the basis of the propagation mechanisms observed, two expressions for the Energy Release Rate have been defined for the prediction of the crack growth rate by means of Paris-like laws. In particular, G_I is only used for low values of *MM* (Mode I dominated loadings), whereas an expression based on the maximum principal stress distribution at the crack tip in the matrix is used for higher values of mode-mixity. The introduction of these parameters allowed the crack growth rate data to be collapsed into two Paris-like scatter bands covering the whole mode-mixity range.

The model has been validated using crack growth data obtained from literature for a range of materials and geometries (i.e. off-axis cracks in glass-epoxy tubes, delamination in glass-epoxy and carbon-epoxy laminates). Furthermore, the transition between the two dominant propagation modes was found to occur for similar values of the mode-mixity for all the conditions analysed.

The proposed crack growth model along with the analytical multiscale approach constitutes a new methodology to predict off-axis crack propagation for the entire range of mode-mixities in a computationally efficient manner. Off-axis crack propagation under mixed-mode conditions plays an important role in the damage evolution process of FRP laminates subjected to multiaxial fatigue loading. Therefore, the new modelling approach represents a key component of future damage-based multiaxial fatigue models for FRP laminates.

7. Acknowledgements

The work presented was conducted as a part of a Ph.D. project at the Department of Mechanical and Manufacturing Engineering, Aalborg University, Denmark. A part of the research was carried out during a visit of the corresponding author to the Department of Management and Engineering, University of Padova, Italy. The project has received sponsorship from Innovation Fund Denmark through the "Danish Centre for Composite Structures and Materials for Wind Turbines (DCCSM)". The support received is gratefully acknowledged.

Glud, J.A., Carraro, P.A., Quaresimin, M., Dulieu-Barton, J.M., Thomsen, O.T. and Overgaard, L.C.T., "A damage-based model for mixed-mode crack propagation in composite laminates", Composites A, 107, 2018, 421-431. https://doi.org/10.1016/j.compositesa.2018.01.016

References

[1] Quaresimin M, Susmel L, Talreja R. Fatigue behaviour and life assessment of composite laminates under multiaxial loadings. Int J Fatigue 2010;32:2–16. doi:10.1016/j.ijfatigue.2009.02.012.

[2] Tong J, Guild FJ, Ogin SL, Smith PA. On matrix crack growth in quasi-isotropic laminates - I. Experimental investigation. Compos Sci Technol 1997;57:1527–35. doi:10.1016/s0266-3538(97)00080-8.

[3] Wharmby AW, Ellyin F. Damage growth in constrained angle-ply laminates under cyclic loading. Compos Sci Technol 2002;62:1239–47. doi:10.1016/s0266-3538(02)00075-1.

[4] Adden S, Horst P. Stiffness degradation under fatigue in multiaxially loaded non-crimped-fabrics. Int J Fatigue 2010;32:108–22. doi:10.1016/j.ijfatigue.2009.02.002.

[5] Quaresimin M, Carraro PA. Damage initiation and evolution in glass/epoxy tubes subjected to combined tension-torsion fatigue loading. Int J Fatigue 2014;63:25–35. doi:10.1016/j.ijfatigue.2014.01.002.

[6] Carraro PA, Quaresimin M. A stiffness degradation model for cracked multidirectional laminates with cracks in multiple layers. Int J Solids Struct 2015;58:34–51. doi:10.1016/j.ijsolstr.2014.12.016.

[7] Quaresimin M, Carraro PA, Maragoni L. Early stage damage in off-axis plies under fatigue loading. Compos Sci Technol 2016;128:147–54. doi:10.1016/j.compscitech.2016.03.015.

[8] Carraro PA, Quaresimin M. A damage based model for crack initiation in unidirectional composites under multiaxial cyclic loading. Compos Sci Technol 2014;99:154–63. doi:10.1016/j.compscitech.2014.05.012.

[9] Benzeggagh ML, Kenane M. Measurement of mixed-mode delamination fracture toughness of unidirectional glass/epoxy composites with mixed-mode bending apparatus. Compos Sci Technol 1996;56:439–49. doi:10.1016/0266-3538(96)00005-X.

[10] Kenane M, Benzeggagh ML. Mixed-mode delamination fracture toughness of unidirectional glass/epoxy composites under fatigue loading. Compos Sci Technol 1997;57:597–605.

doi:10.1016/S0266-3538(97)00021-3.

[11] Liu Z, Gibson RF, Newaz GM. The use of a modified mixed mode bending test for characterization of mixed-mode fracture behavior of adhesively bonded metal joints. J Adhes 2010;78:223–44. doi:10.1080/00218460210408.

[12] Cheuk P., Tong L, Wang C., Baker A, Chalkley P. Fatigue crack growth in adhesively bonded composite-metal double-lap joints. Compos Struct 2002;57:109–15. doi:10.1016/S0263-8223(02)00074-0.

[13] Hafiz TA, Abdel Wahab MM, Crocombe AD, Smith PA. Mixed-mode fracture of adhesively bonded metallic joints under quasi-static loading. Eng Fract Mech 2010;77:3434–45. doi:10.1016/j.engfracmech.2010.09.015.

[14] Hafiz TA, Abdel-Wahab MM, Crocombe AD, Smith PA. Mixed-mode fatigue crack growth in FM73 bonded joints. Int J Adhes Adhes 2013;40:188–96. doi:10.1016/j.ijadhadh.2012.07.004.

[15] Bak BL V., Sarrado C, Turon A, Costa J. Delamination under fatigue loads in composite laminates: a review on the observed phenomenology and computational methods. Appl Mech Rev 2014;66:60803. doi:10.1115/1.4027647.

[16] Carraro PA, Meneghetti G, Quaresimin M, Ricotta M. Crack propagation analysis in composite bonded joints under mixed-mode (I+II) static and fatigue loading: experimental investigation and phenomenological modelling. J Adhes Sci Technol 2013;27:1179–96. doi:10.1080/01694243.2012.735902.

[17] Armanios E, Bucinell R, Wilson D, Asp L, Sjögren A, Greenhalgh E. Delamination growth and thresholds in a carbon/epoxy composite under fatigue loading. J Compos Technol Res 2001;23:55. doi:10.1520/CTR10914J.

[18] Carraro PA, Meneghetti G, Quaresimin M, Ricotta M. Crack propagation analysis in composite bonded joints under mixed-mode (I+II) static and fatigue loading: a damage-based model. J Adhes Sci Technol 2013;27:1393–406. doi:10.1080/01694243.2012.735901.

[19] Bürger D, Rans CD, Benedictus R. Influence of fabric carrier on the fatigue disbond behavior of metal-to-metal bonded interfaces. J Adhes 2013.

[20] Wang CH. Fracture of interface cracks under combined loading. Eng Fract Mech 1997;56:77–86. doi:10.1016/S0013-7944(96)00111-7.

[21] Purslow D. Matrix fractography of fibre-reinforced epoxy composites. Composites 1986;17:289–303. doi:10.1016/0010-4361(86)90746-9.

[22] Sih GC, Paris PC, Irwin GR. On cracks in rectilinearly anisotropic bodies. Int J Fract Mech 1965;1. doi:10.1007/BF00186854.

[23] Ho S, Suo Z. Tunneling cracks in constrained layers. J Appl Mech 1993;60:890. doi:10.1115/1.2900998.

[24] Quaresimin M, Carraro PA, Mikkelsen LP, Lucato N, Vivian L, Brøndsted P, et al. Damage evolution under cyclic multiaxial stress state: A comparative analysis between glass/epoxy laminates and tubes. Compos Part B Eng 2014;61:282–90. doi:10.1016/j.compositesb.2014.01.056.

[25] Bürger D. Mixed-mode fatigue disbond on metallic bonded joints, PhD dissertation. Delft University of Technology, 2015.

[26] Quaresimin M, Carraro PA, Maragoni L. Influence of load ratio on the biaxial fatigue behaviour and damage evolution in glass/epoxy tubes under tension–torsion loading. Compos Part A Appl Sci Manuf 2015;78:294–302. doi:10.1016/j.compositesa.2015.08.009.

[27] Tanaka H, Tanaka K, Tsuji T, Katoh H. Mixed-mode (I+II) propagation of delamination fatigue cracks in unidirectional graphite/epoxy laminates. Trans Japan Soc Mech Eng Ser A 1999;65:1676–83. doi:10.1299/kikaia.65.1676.

[28] Murri GB. Evaluation of delamination onset and growth characterization methods under mode I fatigue loading, NASA/TM–2013-217966. Hampton: 2013.

[29] O'Brien TK, Johnston WM, Toland GJ. Mode II interlaminar fracture toughness and fatigue characterization of a graphite epoxy composite material, NASA/TM–2010-216838. Hampton: 2010.

Glud, J.A., Carraro, P.A., Quaresimin, M., Dulieu-Barton, J.M., Thomsen, O.T. and Overgaard, L.C.T., “A damage-based model for mixed-mode crack propagation in composite laminates”, Composites A, 107, 2018, 421-431. https://doi.org/10.1016/j.compositesa.2018.01.016

[30] Ratcliffe JG, Johnston, William M. J. Influence of mixed mode I-mode II loading on fatigue delamination growth characteristics of a graphite epoxy tape laminate. Proc. 29th ASC Tech. Conf., San Diego, La Jolla, CA: 2014.

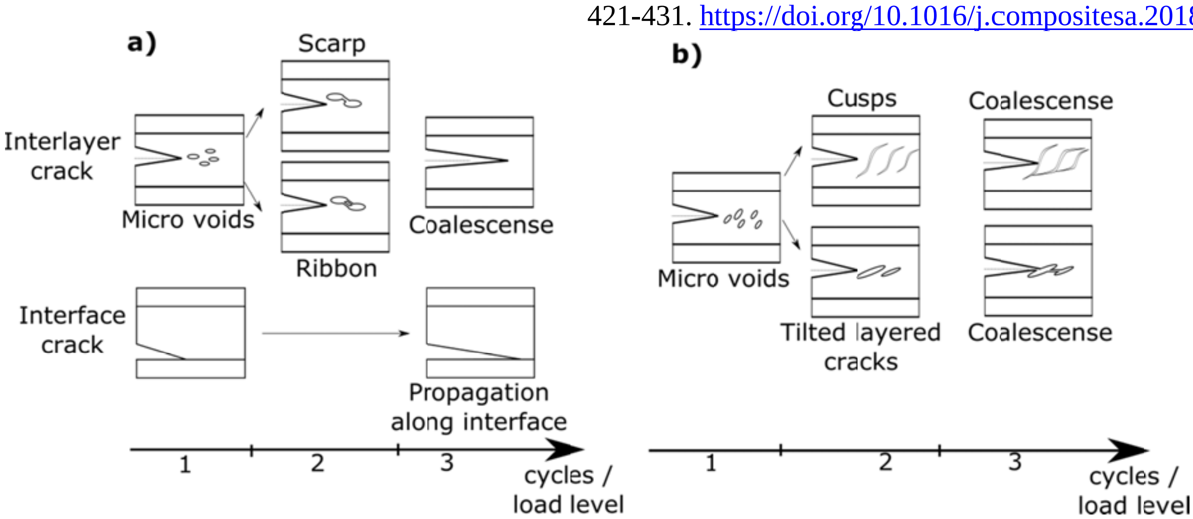

Figure 1: Reported damage sequence for a) Mode I dominated loading and b) Mode II dominated loading.

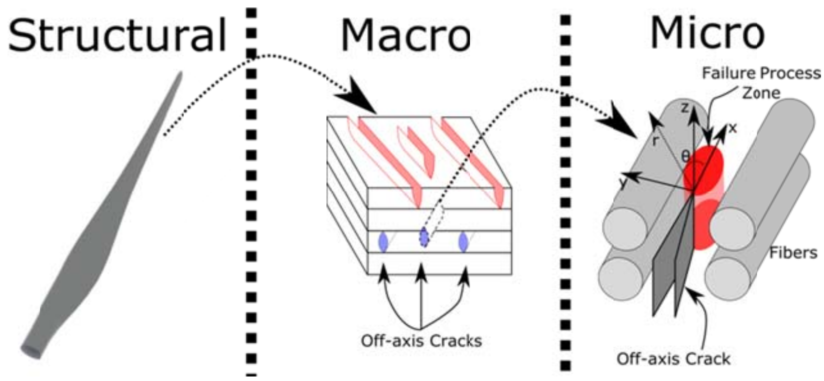

Figure 2: Multiple scales in off-axis crack propagation.

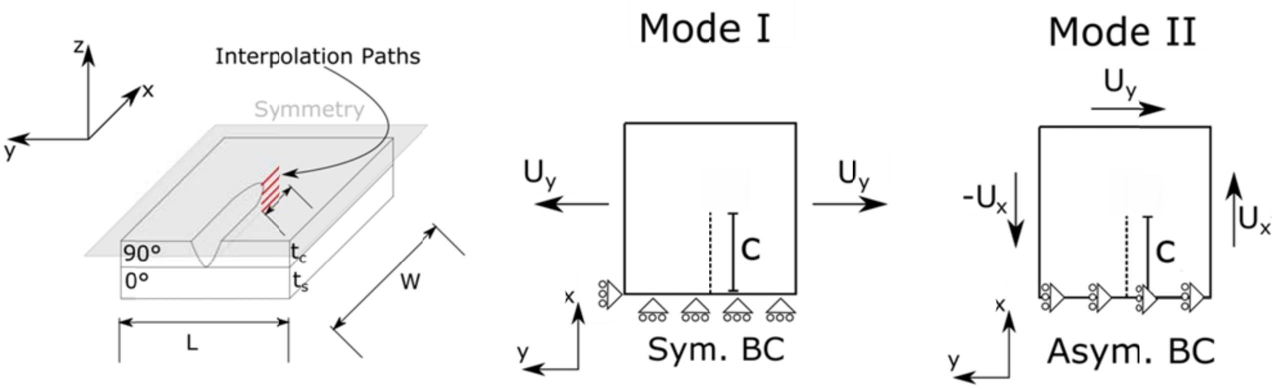

Figure 3: 3D unit-cell model to study stress state ahead of the off-axis crack tip with imposed displacement boundary conditions for Mode I and Mode II loading. U_x and U_y are displacements applied to all nodes at the corresponding edge and c is the length of the modelled crack.

Glud, J.A., Carraro, P.A., Quaresimin, M., Dulieu-Barton, J.M., Thomsen, O.T. and Overgaard, L.C.T., “A damage-based model for mixed-mode crack propagation in composite laminates”, Composites A, 107, 2018, 421-431. https://doi.org/10.1016/j.compositesa.2018.01.016

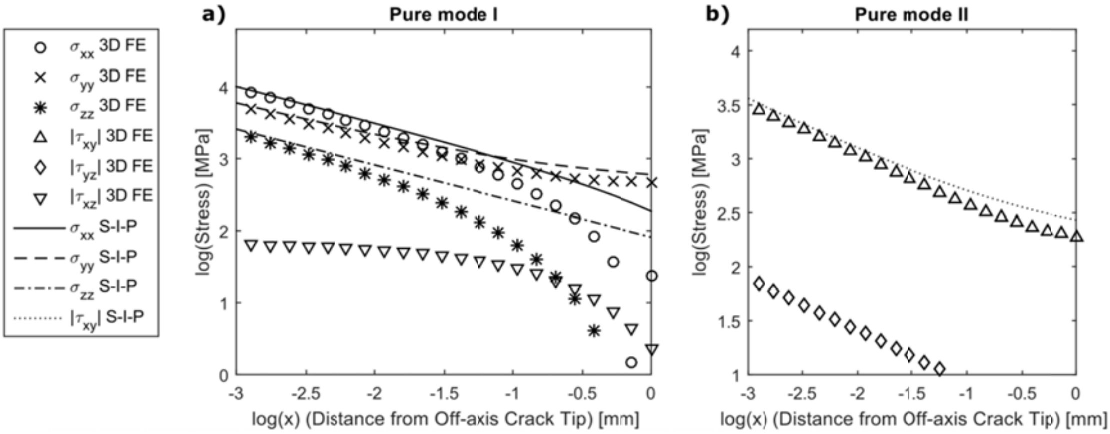

Figure 4: Average through-thickness stress state on the crack plane in front of the off-axis crack tip when loaded in a) Mode I and b) Mode II.

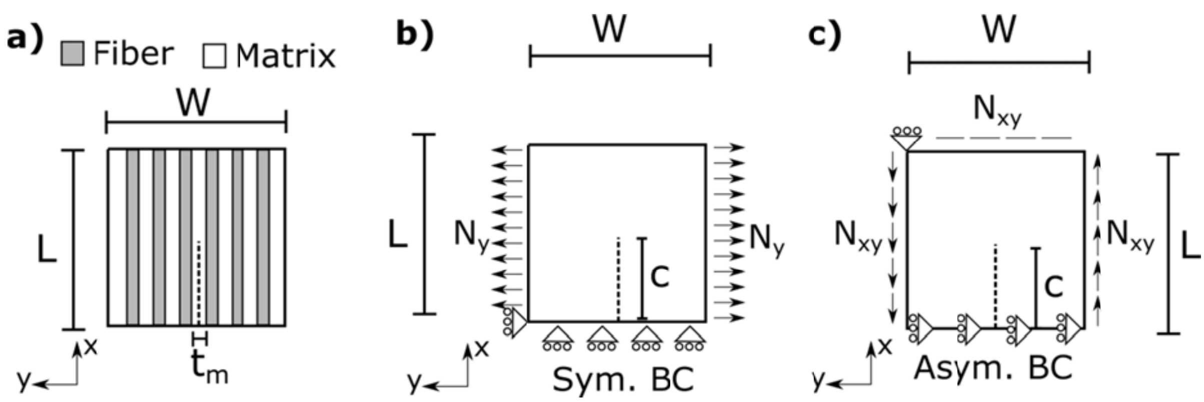

Figure 5: a) Plate model used for studying the influence of crack length in a heterogeneous material; b) Mode I loading condition and c) Mode II loading; $N_y = N_{xy} = 50$ N/mm

Glud, J.A., Carraro, P.A., Quaresimin, M., Dulieu-Barton, J.M., Thomsen, O.T. and Overgaard, L.C.T., "A damage-based model for mixed-mode crack propagation in composite laminates", Composites A, 107, 2018, 421-431. https://doi.org/10.1016/j.compositesa.2018.01.016

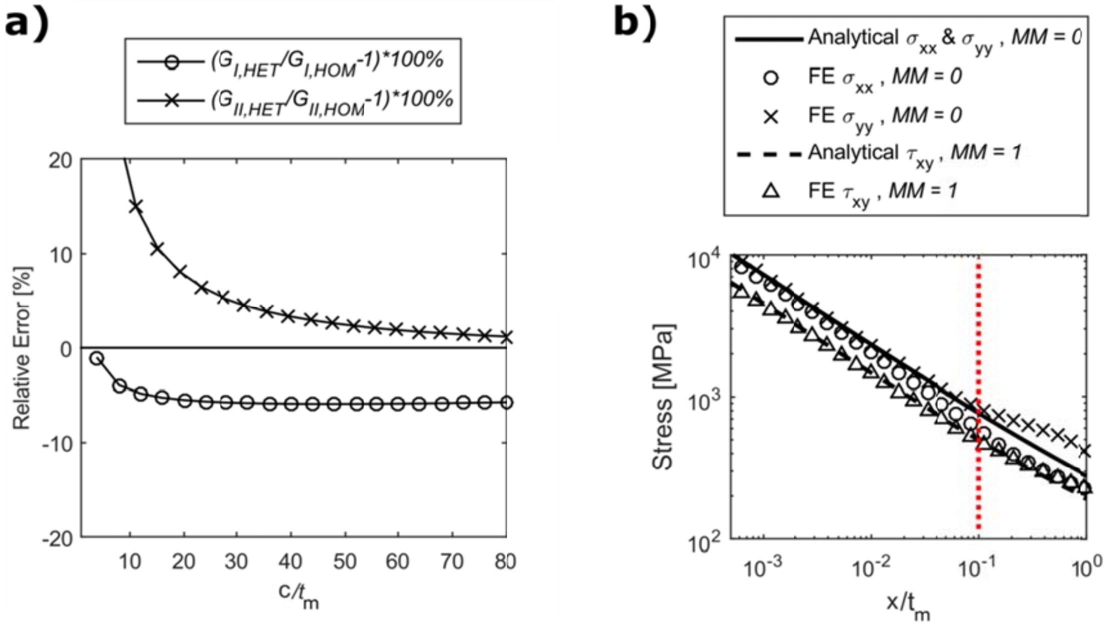

Figure 6: a) Relative error for the ERR between homogeneous and heterogeneous material and b) matrix stress state in the vicinity of the crack tip.

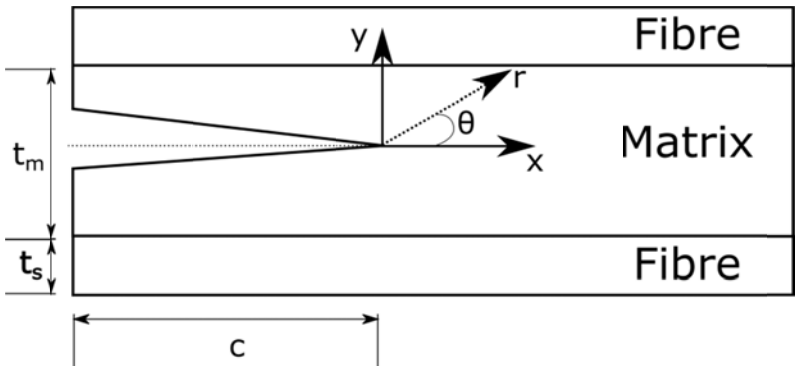

Figure 7: Schematic of an interfacial crack within the matrix material.

Glud, J.A., Carraro, P.A., Quaresimin, M., Dulieu-Barton, J.M., Thomsen, O.T. and Overgaard, L.C.T., "A damage-based model for mixed-mode crack propagation in composite laminates", Composites A, 107, 2018, 421-431. https://doi.org/10.1016/j.compositesa.2018.01.016

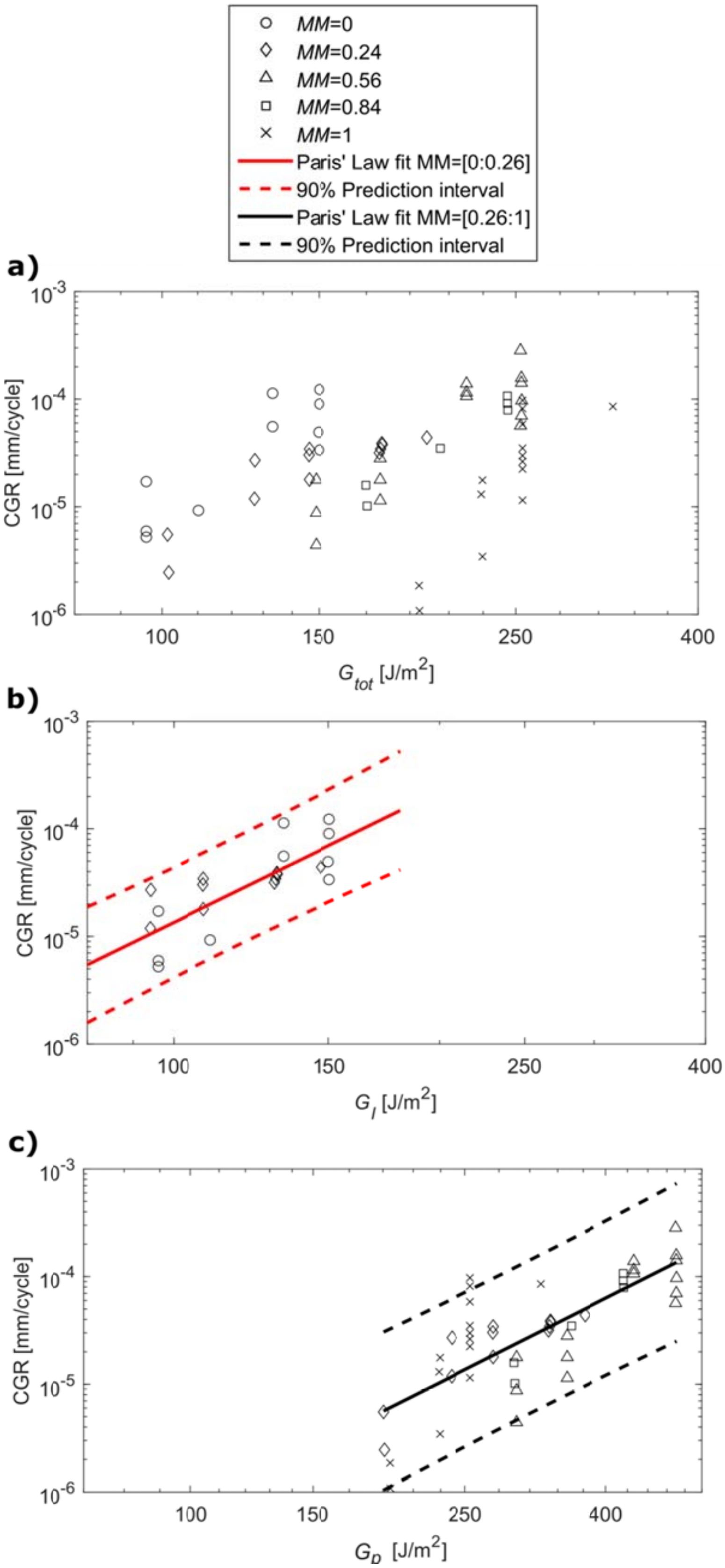

Figure 8: CGR data for off-axis cracks in glass-epoxy tubes *[5]*. a) CGR data plotted as function of G_{tot}, b) G_I (*MM*=[0:0.24]) and c) G_p (*MM*=[0.24:1]).

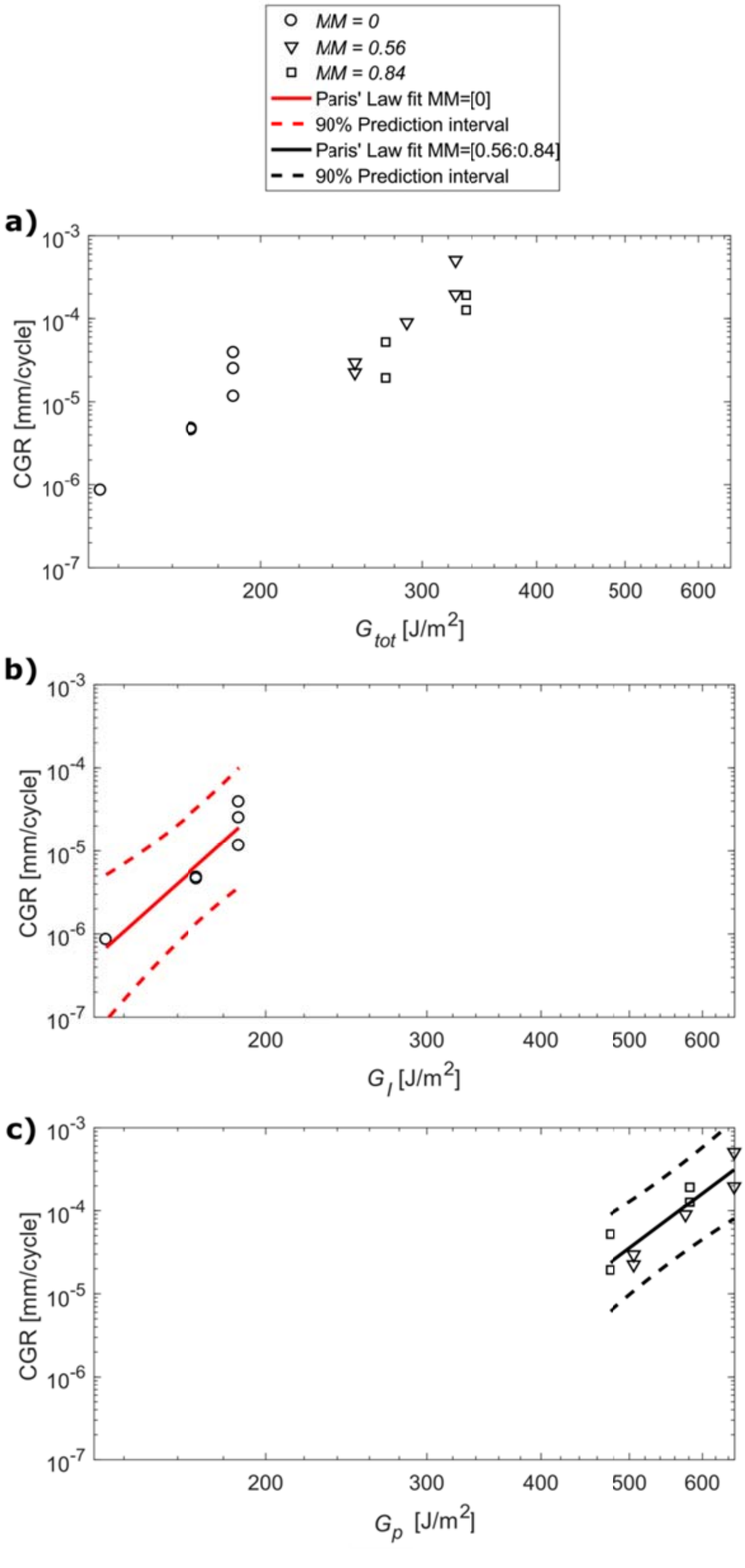

Figure 9: CGR data for off-axis cracks in glass-epoxy tubes for a load-ratio of R=0.5 *[26]*. a) CGR data plotted as function of G_{tot}, b) G_I (MM=[0]) and c) G_p (MM=[0.56:0.84]).

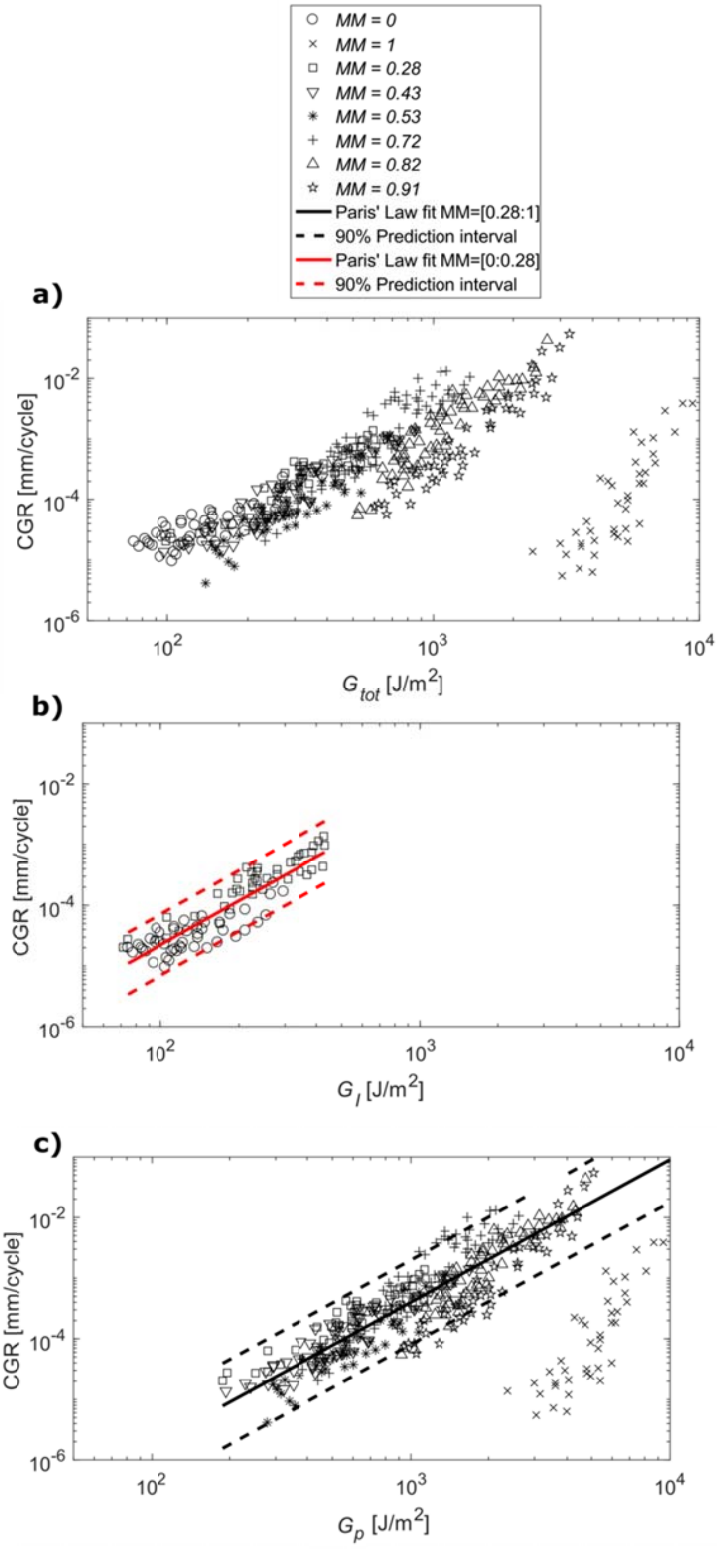

Figure 10: CGR data for delaminations in a 0°/0° interface in glass-epoxy laminates *[10]* as function of a) G_{tot}, b) G_I (*MM*=[0:0.28]) and c) G_p (*MM*=[0.28:1]).

Glud, J.A., Carraro, P.A., Quaresimin, M., Dulieu-Barton, J.M., Thomsen, O.T. and Overgaard, L.C.T., "A damage-based model for mixed-mode crack propagation in composite laminates", Composites A, 107, 2018, 421-431. https://doi.org/10.1016/j.compositesa.2018.01.016

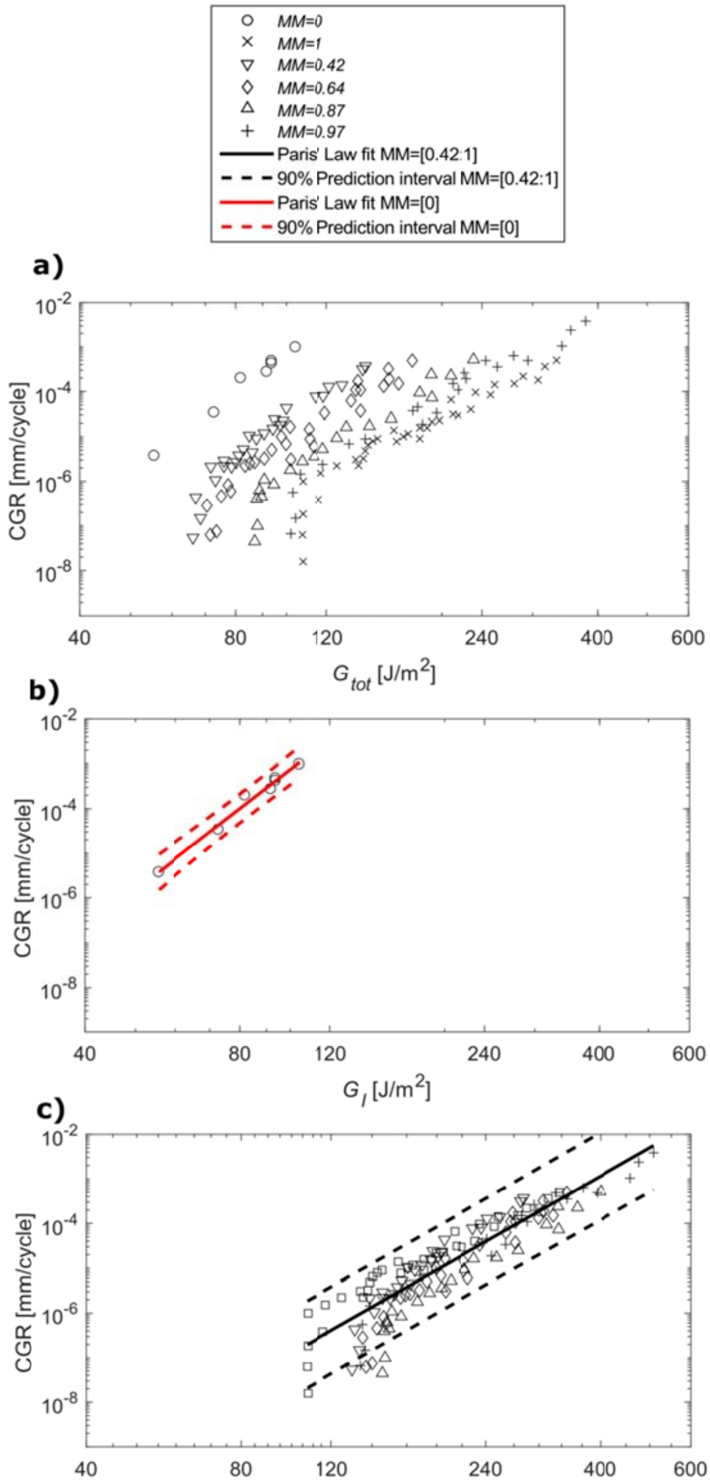

Figure11: CGR data for delamination in a 0°/0° interface in graphite-epoxy laminates *[27]* as function of a) G_{tot}, b) G_I (MM=0) and c) G_p (MM=[0.42:1]).

Glud, J.A., Carraro, P.A., Quaresimin, M., Dulieu-Barton, J.M., Thomsen, O.T. and Overgaard, L.C.T., "A damage-based model for mixed-mode crack propagation in composite laminates", Composites A, 107, 2018, 421-431. https://doi.org/10.1016/j.compositesa.2018.01.016

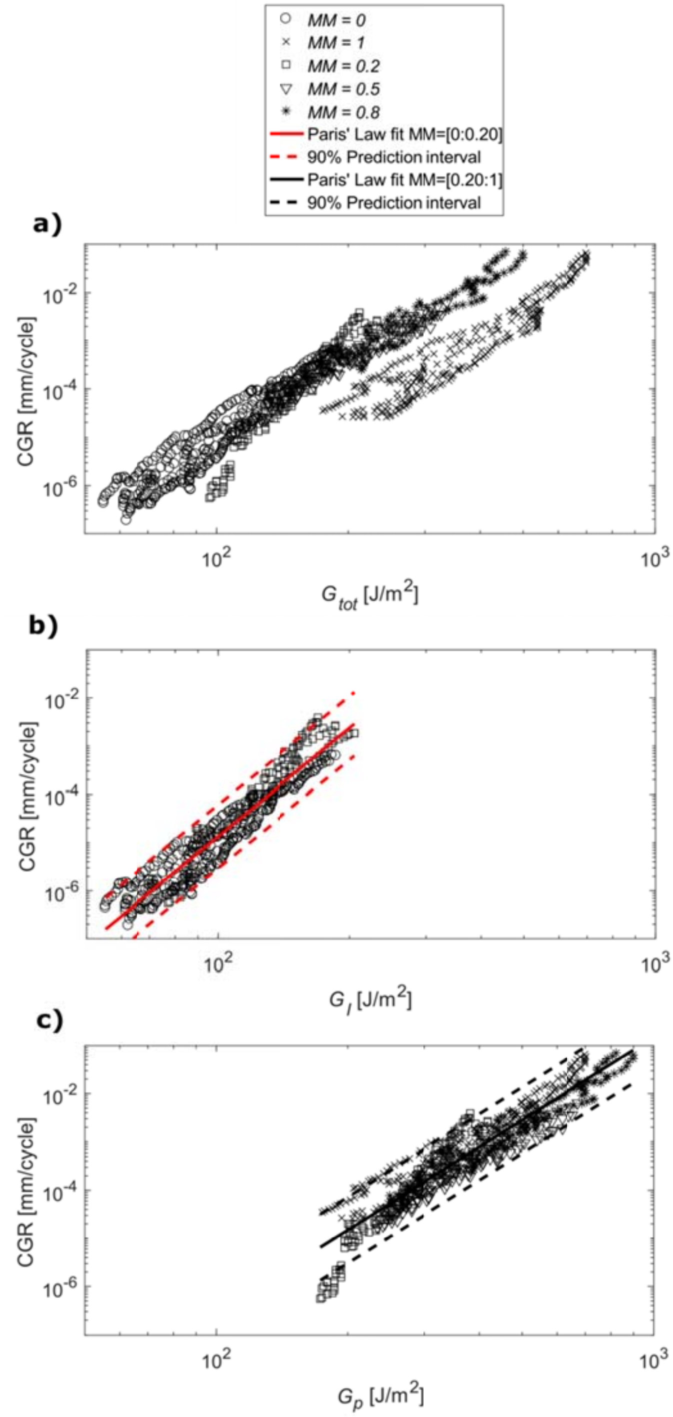

Figure 12: CGR data for delaminations in a 0°/0° interface in carbon-epoxy laminates *[28–30]* as function of a) G_{tot}, b) G_I (*MM*=[0:0.2]) and c) G_p (*MM*=[0.2:1]).

Glud, J.A., Carraro, P.A., Quaresimin, M., Dulieu-Barton, J.M., Thomsen, O.T. and Overgaard, L.C.T., "A damage-based model for mixed-mode crack propagation in composite laminates", Composites A, 107, 2018, 421-431. https://doi.org/10.1016/j.compositesa.2018.01.016

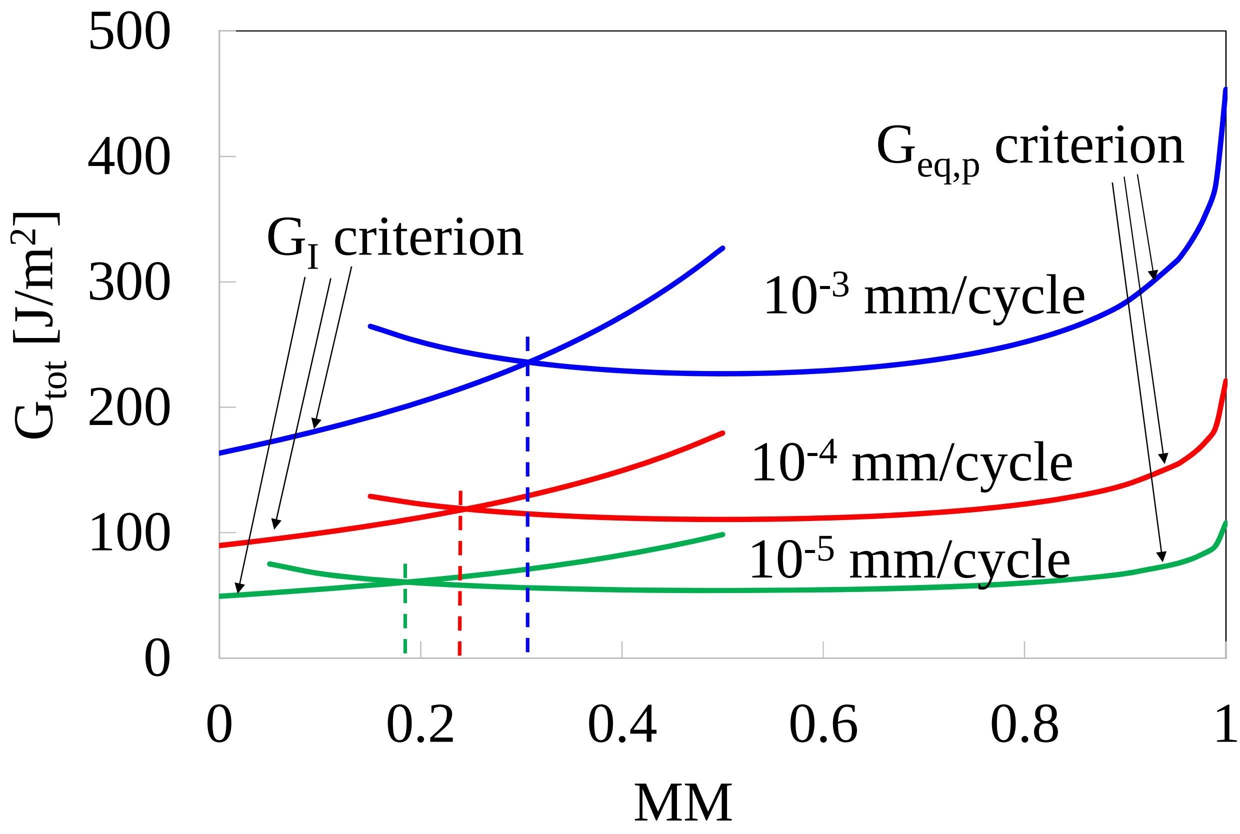

Figure 13: Constant-CGR plots for the glass/epoxy material adopted in Ref. [5]